MATERIALS CHEMISTRY
FRONTIERS

RESEARCH ARTICLE

View Article Online
View Journal | View Issue

Cite this: *Mater. Chem. Front.*, 2018, **2**, 1343

Short-wave infrared emitted/excited fluorescence from carbon dots and preliminary applications in bioimaging†

Dongyu Li,[a] Dan Wang,*[b] Xinyuan Zhao,[c] Wang Xi,[d] Abudureheman Zebibula,[d] Nuernisha Alifu,[a] Jian-Feng Chen[b] and Jun Qian *[a]

Received 6th April 2018,
Accepted 9th May 2018

DOI: 10.1039/c8qm00151k

rsc.li/frontiers-materials

Fluorescent carbon dots (FCDs) have attracted tremendous attention in biological applications. The short-wave infrared (SWIR, 900–1700 nm) spectral range is considered as a novel optical tissue window due to low photon scattering. In this work, we investigated the fluorescence characteristics of FCDs based on the SWIR spectral range. SWIR emissions were observed from FCDs for the first time, when long-wavelength excitation (*e.g.* longer than 731 nm) was adopted. Wavelength-tunable two-photon fluorescence could also be obtained from the FCDs, under 1000–1560 nm SWIR femtosecond (fs) excitation. Interestingly, when an fs excitation wavelength as long as 1560 nm was adopted, two typical nonlinear optical signals, namely two-photon fluorescence and third harmonic generation (THG), could be observed. Based on the one-photon SWIR fluorescence, FCDs were successfully utilized for *in vivo* sentinel node mapping and tumour imaging. Under SWIR fs excitation, FCD-assisted two-photon fluorescence microscopy realized deep-tissue imaging of zebrafish embryos and the brain neuron networks of mice. SWIR excited and emitting FCDs have potential as fluorescent probes for deep-tissue and high-contrast functional bioimaging and related applications in the future.

Introduction

Carbon dots (CDs), also known as carbon quantum dots or carbon nanodots, generally refer to small carbon nanoparticles with a typical size under 10 nm in all three dimensions.[1] Among the most important features of CDs, fluorescence is of particular interest, which makes them useful in various applications,[2,3] such as photovoltaic devices,[4] light-emitting diodes,[5] and biological diagnosis and therapy.[6–9]

The one-photon fluorescence of CDs usually exhibits an excitation-dependent feature, enabling multi-color fluorescence detection for biological imaging.[10] However, in most of the previous literature, the fluorescence wavelength of CDs is usually in the visible spectral range,[11–15] while the emission behaviour of CDs in the traditional near-infrared spectral region (NIR, 700–900 nm) has seldom been reported,[16] let alone fluorescence in the short-wave infrared (SWIR) spectral range (900–1700 nm). As we known, penetration of visible light into biological tissues is quite limited because of the large photon absorption and scattering, which results in a distinct photon attenuation and is unfavourable for deep-tissue fluorescence imaging. The traditional NIR region (700–900 nm) is a typical optical tissue window due to low photon absorption in biological tissues. Recently, the SWIR spectral range has been considered as another novel optical tissue window, because although the photon absorption is a little bit high in this window, the photon scattering is low due to the increased wavelength. Fluorescence signals with low photon scattering have reduced attenuation and optical diffusion.[17] In addition, SWIR autofluorescence from biological tissues is not as intense.[18] Thus, SWIR fluorescence imaging allows deep-tissue bioimaging with high spatial resolution and signal to noise ratio.[19–21]

Two-photon fluorescence is a process in which a fluorophore simultaneously absorbs two photons with a long wavelength and emits fluorescence with a short wavelength afterwards.[22] The wavelength of the femtosecond (fs) excitation laser for two-photon fluorescence is usually in the traditional NIR region

[a] *State Key Laboratory of Modern Optical Instrumentations, Center for Optical and Electromagnetic Research, JORCEP (Sino-Swedish Joint Research Center of Photonics) Zhejiang University, Hangzhou 310058, China. E-mail: qianjun@zju.edu.cn*
[b] *State Key Laboratory of Organic–Inorganic Composites, Beijing University of Chemical Technology, Beijing 100029, China. E-mail: wangdan@mail.buct.edu.cn*
[c] *Department of Occupational Medicine and Environmental Toxicology, School of Public Health, Nantong University, Nantong, 226001, China*
[d] *Department of Urology, Sir Run-Run Shaw Hospital College of Medicine, Zhejiang University, Hangzhou 310016, China*

† Electronic supplementary information (ESI) available: Characterization of FCDs; schematic illustration of the setup for one/two-photon fluorescence spectra measurement and imaging; cell toxicity of FCDs; two-photon fluorescence imaging of cells and zebrafish. See DOI: 10.1039/c8qm00151k

(700–900 nm) with a low photon absorption. Thus, two-photon fluorescence microscopy is beneficial to realize deep-tissue bioimaging due to low photon attenuation of the excitation light.[23–27] The application of CDs as nanoprobes for two-photon fluorescence imaging of cells and tissues has emerged as a hot topic in recent years.[28–34] However, as far as we know, two-photon fluorescence features of CDs under SWIR fs excitation have never been reported. SWIR excitation light has reduced photon scattering, and it can penetrate deeper and focus more tightly in biological tissues than that in the traditional NIR region.[35,36] Thus, SWIR fs excited two-photon fluorescence microscopy can realize *in vivo* visualization with a larger image depth.

In this present work, we synthesized fluorescent carbon dots (FCDs) through a commonly used approach, by hydrothermal carbonization of citric acid and ethylenediamine.[37] The excitation-dependent (one-photon) fluorescence from the FCDs was measured. SWIR fluorescence from the FCDs was observed for the first time when the excitation wavelength of the continuous wave (CW) laser was longer than 731 nm, and the SWIR fluorescence exhibited a broad shoulder with a spectral tail extending to as long as 1500 nm. Wavelength-tunable two-photon fluorescence was also obtained from the FCDs, by utilizing SWIR fs excitation from 1000 nm to 1560 nm. Under the excitation of a 1560 nm fs laser, two types of nonlinear optical signals, namely NIR two-photon fluorescence (centered at 820 nm) and third harmonic generation (THG, centered at 520 nm), could be observed. Based on these findings, FCDs were then used for SWIR fluorescence bioimaging. *In vivo* sentinel node mapping and tumour imaging were successfully demonstrated. In addition, SWIR fs excited two-photon fluorescence imaging towards zebrafish embryos and the brain neuron networks of mice was performed, by using the FCDs as nanoprobes.

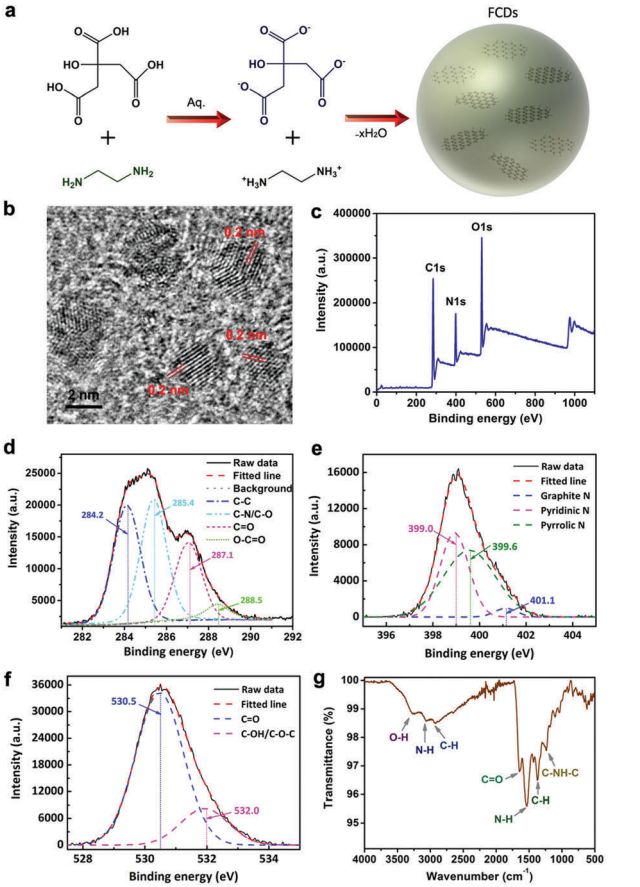

Fig. 1 (a) Scheme illustrating the synthesis process of FCDs. (b) A typical HRTEM image of FCDs. (c) XPS scanning spectrum of FCDs. (d) XPS high resolution survey scan of C 1s. (e) XPS high resolution survey scan of N 1s. (f) XPS high resolution survey scan of O 1s. (g) FTIR spectrum of FCDs.

Results and discussion

Preparation and characterization of FCDs

The formation of FCDs by hydrothermal treatment of citric acid and ethylenediamine is illustrated in Fig. 1a. The reactants were firstly condensed to form polymer-like organic dots and then carbonized to nanosized carbon dots. A typical TEM image showed a uniform distribution of FCDs (Fig. S1, ESI†), and the hydrodynamic size of the FCDs was measured by dynamic light scattering (DLS), which showed an average diameter of 4.2 nm (Fig. S2, ESI†). The HRTEM results shown in Fig. 1b presented the crystalline structure of the FCDs with a lattice spacing of 0.2 nm, which was in agreement with the (102) facet of graphite.[38] The structure and composition of the FCDs were characterized *via* X-ray photoelectron spectroscopy (XPS) and Fourier transform infrared (FTIR) spectroscopy. The XPS spectrum shown in Fig. 1c clearly revealed that carbon, nitrogen and oxygen were present at the surface of the FCDs, with atomic percentages of 61.8%, 22.6% and 15.6%, respectively. The C 1s peaks at 284.2 eV, 285.4 eV, 287.1 eV and 288.5 eV in the expanded XPS spectra (Fig. 1d) could be assigned to carbon in the form of C–C (sp^3), C–N (sp^3), C═O (sp^2), and O–C═O (sp^2) respectively.[39] In addition, the high-resolution XPS survey scan of O 1s and N 1s was measured as well. The N 1s spectrum (Fig. 1e) showed three peaks at 399.0, 399.6 and 401.1 eV, which were attributed to the pyridinic N, pyrrolic N and graphite N, respectively.[40] The O 1s spectrum (Fig. 1f) exhibited two peaks at 530.5 and 532.0 eV, which were attributed to the C═O and C–OH/C–O–C groups, respectively.[41] The characteristic peaks of –COOH (3430 cm^{-1} and 1635 cm^{-1}), –NH (1570 cm^{-1}) and C–NH–C (1126 cm^{-1}) were also observed in the FTIR spectra of FCDs (Fig. 1g).[15] The XRD patterns of the FCDs displayed a broad peak centered at 23°, which was attributed to the highly disordered carbon atoms (Fig. S3, ESI†). Moreover, Raman spectra were collected on a Renishaw invia reflex Raman spectrometer using a 514 nm and a 785 nm wavelength laser as the excitation sources, respectively. The D band (1350 cm^{-1}) and G band (1598 cm^{-1}) were not obvious due to the bright fluorescence of the FCDs, which might disturb the Raman characterization[42] (Fig. S4, ESI†). Due to the abundant hydrophilic groups on the FCDs, the FCD powder could be well dispersed in aqueous solution (inset of Fig. S5, left, ESI†). The absorbance spectrum of the FCDs in the range of 230–700 nm was measured, exhibiting a distinct peak at 330 nm and a shoulder peak at 250 nm (Fig. S5, ESI†), which were attributed to the n–π* transition of the carbonyl

bond and the π–π* transition of the nitrogen heterocyclic sp^2 moieties, respectively. An aqueous dispersion of FCDs showed bright blue emission under the excitation of a 365 nm UV lamp (inset of Fig. S5, right, ESI†), with the emission peak located at 455 nm (Fig. S5, excitation wavelength: 405 nm, ESI†). These results were consistent with those of FCDs obtained by hydrothermal carbonization approaches in previous literature reports.[37] Furthermore, the emission intensities of the FCDs in aqueous dispersions with the same concentration but different pH values (from pH = 4 to pH = 10) were recorded at various time points. As shown in Fig. S6 (ESI†), the variations in the emission intensities were less than 10% in all experimental conditions even after 24 h (normalized by the emission intensity of the dispersion at pH = 7 and 0 h), indicating that the FCDs were stable in various chemical environments. The cytotoxicity studies on the FCDs through an MTT assay revealed that the as-synthesized FCDs were biocompatible to cells even when their concentration was increased to 300 μg mL^{-1} (Fig. S7, ESI†).

Fluorescence from FCDs in the SWIR spectral range

When the excitation wavelength was tuned from 400 to 731 nm, the excitation-dependent emission of the FCDs was observed. The peak fluorescence wavelengths were from 473 nm to 750 nm (Fig. S8, ESI†), mainly distributed in the visible spectral range. However, the peak fluorescence wavelength no longer increased when the excitation wavelength went on increasing (Fig. 2a). These results have also been reported in many previous literature reports.[12,37,43–45] Interestingly, the FCDs exhibited emissions in the SWIR spectral region, when the excitation wavelength was longer than 731 nm (Fig. 2b), and the fluorescence had a broad shoulder with a spectral tail extending to 1500 nm (Fig. 2a). To the best of our knowledge, this phenomenon has never been observed. As previously reported, FCDs always possess excitation wavelength dependent fluorescence, which is attributed to the multiple excited states. Thanks to the broad wavelength coverage, the fluorescence of FCDs could reach the SWIR region when excited by red/NIR light. However, since the SWIR fluorescence of FCDs is rather weak, traditional silicon based detectors (usually adopted in previous research studies on FCDs) could not detect it. Herein, thanks to the SWIR sensitive InGaAs based detector, the fluorescence signals of the FCDs beyond 900 nm were effectively recorded and revealed.

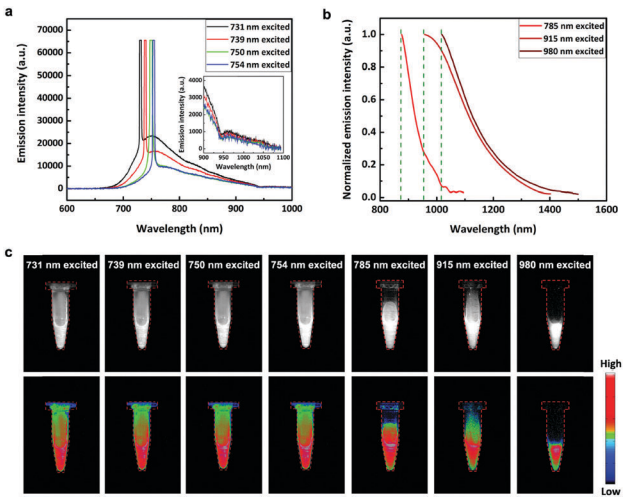

Fig. 2 (a) Fluorescence spectra of FCDs in aqueous dispersion, under the CW excitation of 731 nm, 739 nm, 750 nm and 754 nm CW light, measured using a PG2000 spectrometer. The sharp peaks were the residual laser excitation spectra. (b) SWIR fluorescence spectra of FCDs in aqueous dispersions, under the CW excitation of 785 nm (850 nm long-pass filter added), 915 nm (950 nm long-pass filter added) and 980 nm (1000 nm long-pass filter added), measured by a NIR1700 spectrometer. (c) SWIR fluorescence images of FCDs in aqueous dispersions, excited by 731 nm, 739 nm, 750 nm, 754 nm, 785 nm, 915 nm and 980 nm lasers and captured with an InGaAs camera. Images in the bottom row are the heat maps of those in the upper row.

SWIR fluorescence imaging of an aqueous dispersion of FCDs was then carried on by using CW excitation of 731 nm, 739 nm, 750 nm, 754 nm, 785 nm, 915 nm and 980 nm, and the corresponding images are presented in Fig. 2c. As we can see, the emissions from the FCDs were intense, illustrating that the FCDs could be used as a new type of SWIR fluorescent probe besides carbon nanotubes,[21] quantum dots,[12] rare-earth doped nanoparticles[46] and organic dyes.[19]

FCDs for SWIR fluorescence *in vivo* bioimaging

In view of the advantages of SWIR fluorescence imaging (*e.g.* deep-penetration, high spatial resolution and large signal to noise ratio), as well as the SWIR emission from FCDs, we studied the feasibility of FCDs for SWIR fluorescence biological functional imaging. Fig. 3a shows the mapping of sentinel nodes in a mouse injected with FCDs through the forelegs. Two minutes post treatment, the FCDs already migrated to the sentinel node and emitted SWIR fluorescence signals under 785 nm excitation. The accumulation of FCDs in the sentinel node reached the maximum 10 min post injection. As time went by, the SWIR fluorescence intensity of the FCDs in the sentinel node decreased, indicating that the FCDs were transferred into the circulatory system. The whole process was vividly recorded based on SWIR fluorescence imaging. Further application of FCDs as SWIR nanoprobes for *in vivo* tumour imaging was also achieved. Fig. 3b shows the SWIR images of two subcutaneous tumour bearing mice with intratumour injection of FCDs, by using 915 nm and 980 nm excitation lasers, respectively. The profile of the tumours could be visualized clearly, thanks to the SWIR fluorescence from the FCDs. In addition, under either 915 nm or 980 nm excitation, biological tissues exhibit negligible autofluorescence in the SWIR region, making the images possess high contrast.

Since SWIR fluorescence bioimaging could provide a high spatial resolution and large penetration depth, some fluorescent probes have been developed in recent years. In terms of biocompatibility, organic FCDs are better alternatives compared to some inorganic probes (*e.g.* quantum dots and rare earth doped nanoparticles).[16,47–49] Indeed, the SWIR fluorescence brightness of the existing FCDs is not as high as that of some other reported organic emitters (*e.g.* dyes[19] and aggregation-induced emission (AIE) dots[50]) but there is still plenty of room for improvement in the future. Besides, FCDs possess the advantage of convenient

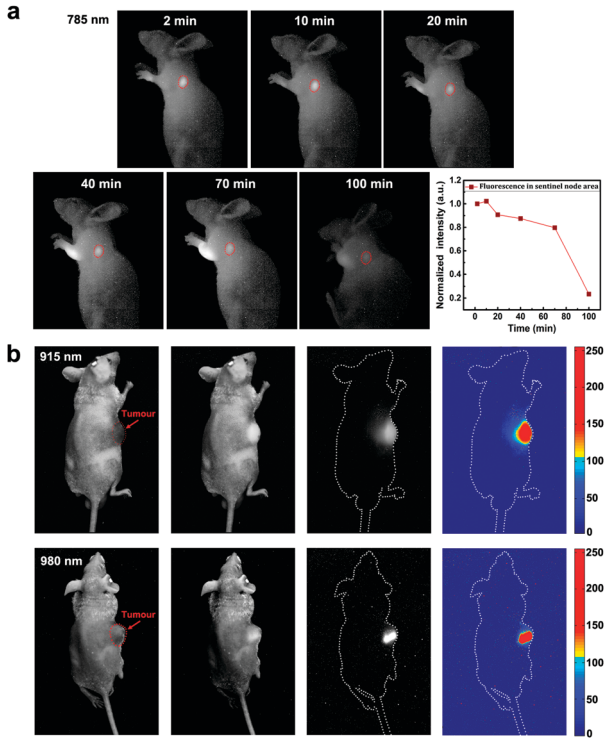

Fig. 3 (a) SWIR fluorescence images of a nude mouse injected with an aqueous dispersion of FCDs in the forefoot, and normalized fluorescence intensities of the sentinel node at various time points. Wavelength of CW excitation: 785 nm. The sentinel node of the mouse in each image was marked with a red circle. (b) SWIR fluorescence images of two mice with intratumour injection of an aqueous dispersion of FCDs. Wavelengths of CW excitation: 915 nm and 980 nm. From left to right: under daylight lamp alone, under daylight lamp and excitation light, under excitation light alone, and heat maps under excitation light alone.

surface modification and have been used for many functional biological applications such as drug delivering[51] and therapy.[52] Thus, FCDs should have potential as superior SWIR probes for functional bioimaging.

Two-photon fluorescence of FCDs excited by an SWIR fs laser

The two-photon fluorescence characteristic of FCDs was also studied. As FCDs exhibited negligible linear absorption in the spectral range of 700–860 nm (Fig. S9, ESI†), an fs laser with tunable wavelengths from 770 nm to 860 nm was used as the excitation source. In this case, the FCDs exhibited excitation-dependent two-photon fluorescence, with peak wavelengths from 500 nm to 550 nm (Fig. S10, ESI†). Furthermore, the fs excitation wavelength was tuned to the SWIR region (*e.g.* from 1000 nm to 1360 nm), in which the FCDs also possessed a high linear transmission. Correspondingly, two-photon fluorescence with a spectral peak from 580 nm to 740 nm was generated from the FCDs (Fig. 4a). Since SWIR light with lower photon scattering can penetrate deeper and focus more tightly in biological tissues, the FCDs may be used as probes for SWIR fs excited two-photon fluorescence microscopy, realizing deep-tissue bioimaging. More interestingly, when excited by a 1560 nm fs laser, two types of nonlinear optical signals could be observed

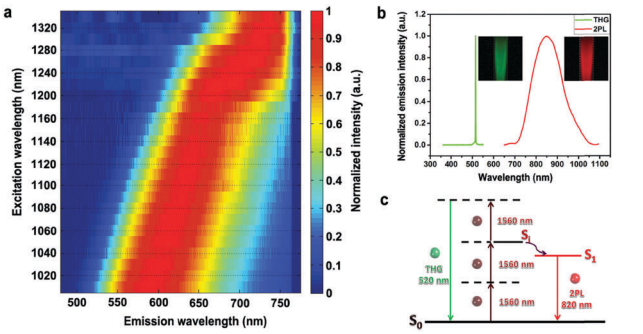

Fig. 4 (a) Two-photon fluorescence spectra of FCDs in an aqueous dispersion, under SWIR fs excitation from 1000 nm to 1360 nm. (b) THG spectrum (green line) and two-photon fluorescence spectrum (red line) of FCDs in an aqueous dispersion, excited by a 1560 nm fs laser. Inset: THG (left) and two-photon fluorescence (right) images of FCDs in an aqueous dispersion, excited by a 1560 nm fs laser. (c) Diagrams showing the proposed generation mechanisms of THG and two-photon fluorescence from FCDs.

from the FCDs (Fig. 4b). One had a sharp peak centered at 520 nm, which was exactly one third of 1560 nm, indicating that it should be third harmonic generation (THG). As we know, FCDs have abundant C=C bonds and C=O bonds to form extended π-conjugation, which helped the FCDs to achieve a distinct nonlinear optical effect (*e.g.* THG).[53] The other was centered at 830 nm, which was close to the peak fluorescence wavelength (750 nm) of FCDs excited by 731 nm CW light, rather than that (610 nm) of FCDs excited by 532 nm CW light. This indicated that this signal was two-photon fluorescence directly excited by the 1560 nm fs excitation instead of one-photon fluorescence excited by the THG signal (Fig. 4c).[27] For most commonly used fluorescent agents, due to the energy band, THG usually appears together with three-photon fluorescence while second harmonic generation (SHG) appears together with two-photon fluorescence.[53–56] However, because of the unique excitation-dependent emission feature, FCDs are capable of producing THG and long-wavelength two-photon fluorescence simultaneously, under SWIR fs excitation with only one wavelength. Just for curiosity, we utilized a short-wavelength (620 nm, shorter than 700 nm) fs laser to excite FCDs, and both "red" one-photon fluorescence and "green" two-photon fluorescence (two emission peaks) could be observed simultaneously (Fig. S11, ESI†). This phenomenon could also be attributed to the excitation-dependent emission feature of FCDs, and has never been observed in other fluorophores before.

FCDs for SWIR excited two-photon fluorescence microscopy

The preliminary applications of FCDs as SWIR fs excited two-photon fluorescent probes for bioimaging were studied. Fig. S12 (ESI†) shows the two-photon fluorescence image of *in vitro* cells incubated with FCDs (100 μg mL^{-1}) for 2 h and excited by a 900 nm fs laser. According to the bright signals from the cytoplasm, FCDs were taken up uniformly by the cells. In addition, the imaging quality was as good as that excited by an 800 nm fs laser, where 800 nm is a commonly used excitation wavelength for two-photon fluorescence imaging.

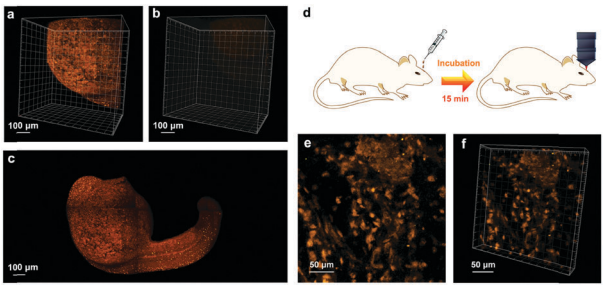

Fig. 5 (a and b) 3D reconstructed two-photon fluorescence images of a part of a zebrafish embryo treated with (a) and without (b) FCDs, under 1040 nm fs excitation. (c) Stacked two-photon fluorescence image of the zebrafish embryo treated with FCDs for 24 hours, under 1040 nm fs excitation. (d) Schematic illustration of the incubation of FCDs with the mouse brain with an open skull. (e) Two-photon fluorescence image of FCD-stained neurons in the brain of a living mouse, under 1040 nm fs excitation. (f) 3D reconstructed two-photon fluorescence image of neurons.

The embryos of zebrafish were used as another model for FCD-based and SWIR-excited two-photon fluorescence bioimaging. The embryos were microinjected with FCDs during the single-cell stage. After incubation for 24 hours, the embryos were imaged with a lab-built two-photon fluorescence scanning microscope equipped with a 1040 nm fs laser. During the imaging process, the 1040 nm fs laser scanned from top to bottom of the embryo, and a single image was obtained at each focal plane. The three-dimensional (3D) reconstructed image is shown in Fig. 5a. Thanks to the two-photon fluorescence from the FCDs, the profile of the fish head could be observed clearly. In contrast, in the zebrafish without the treatment of FCDs, only remarkably weak autofluorescence was observed (Fig. 5b). The images collected from all of the focal planes were then stacked together to form a single picture (Fig. 5c and Fig. S13, ESI†). As FCDs spread over the fish embryo during its growth and development process, the profile of the whole zebrafish could be visualized vividly under the SWIR fs excited two-photon fluorescence microscope. Furthermore, by utilizing FCDs, SWIR excited two-photon fluorescence *in vivo* imaging was performed. As shown in Fig. 5d, FCDs were incubated with the mouse brain for 15 min. After that, the mouse was put under the microscope for observation. As shown in Fig. 5e and f, the neurons emitted distinct two-photon fluorescence under fs excitation of 1040 nm and their morphologies were clearly visualized, indicating that FCDs entered the brain tissues and specifically stained the neurons during the incubation process. As far as we know, this is the first example where FCDs were utilized for intravital brain imaging.

Metabolism and toxicity of FCDs

In order to study the metabolism of the FCDs, they were intravenously injected into mice through the tail vein. The urine and faeces excreted were collected 12 hours after injection. As shown in Fig. S14 and S15 (ESI†), the urine and faeces of the FCD-treated mice showed distinct cyan fluorescence under UV irradiation, indicating that FCDs could be metabolized through both urinary and hepatobiliary transport. 30 days later, the mice were sacrificed to further study the metabolism and the toxicity of the FCDs. The heart, liver, spleen, lungs and kidneys were sliced up and observed under a microscope. The fluorescence microscopic images (Fig. S16, ESI†) showed that FCDs could be hardly detected from the mice viscera, indicating that they were almost metabolized out from the mouse bodies after 30 days. Moreover, the slices were H&E stained and observed using bright-field microscopy, and no noticeable inflammation or abnormalities could be found in the major organs, indicating negligible *in vivo* toxicity of the FCDs towards the mice (Fig. 6).

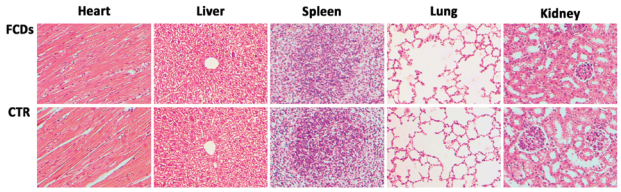

Fig. 6 Microscopic images of the tissue slices of the H&E stained major organs (heart, liver, spleen, lungs and kidneys). Mice were sacrificed 30 days post FCD treatment.

Conclusions

In summary, FCDs have attracted much attention as a class of emerging materials for various applications, particularly in biological diagnosis and therapy. However, among the most important features of FCDs for biological applications, the fluorescence characteristics of FCDs still have not been fully studied. The SWIR spectral region, which ranges from 900 nm to 1700 nm, is considered as a novel optical tissue window due to low photon scattering. In this work, we observed both SWIR emitted (one-photon) and excited (two-photon) fluorescence from FCDs for the first time. In the former case, SWIR fluorescence was excited by the CW-laser with a wavelength longer than 731 nm, and the fluorescence spectrum could extend to as long as 1500 nm. In the latter case, excitation-dependent two-photon fluorescence could be obtained from the FCDs, under the irradiation of a 1000 to 1560 nm SWIR fs laser. Very interestingly, when 1560 nm fs excitation was adopted, green THG and NIR two-photon fluorescence could be observed simultaneously. Based on FCDs, SWIR fluorescence *in vivo* functional bioimaging and SWIR fs excited two-photon fluorescence microscopic bioimaging were successfully demonstrated. Our preliminary study illustrated that SWIR excited and emitting FCDs are promising probes for deep-tissue and high-contrast functional bioimaging and related work in the future.

Experimental section

Materials and instruments

Deuteroxide (D_2O) was purchased from J&K Scientific Co., Ltd, China. Other chemical reagents, which are not specifically mentioned, were purchased from Sigma-Aldrich, Inc. Deionized (DI) water prepared through an Eco-Q15 deionized water system (Shanghai Hitech Instruments Co., Ltd) was used in all the

experimental procedures. The morphology and size distribution of the FCDs were investigated using a high resolution transmission electron microscope (HRTEM, FEI Tecnai G2 F20 S-TWIN, USA) working in bright-field mode. The extinction and transmission spectra were recorded from 200 to 1700 nm with a Shimadzu 3600 UV-vis scanning spectrophotometer at room temperature. PerkinElmer spectrum GX Fourier transform infrared (FTIR) spectroscopy was performed to record the FTIR spectra of the CDs. X-ray photoelectric spectroscopy (XPS) analyses were carried out on a VG Microtech ESCA 2000 using a monochromic Al X-ray source. The X-ray diffraction (XRD) was measured on a Miniflex II Desktop X-ray diffractometer. The Raman spectra were obtained using a Raman spectrometer (Renishaw) with a 514 nm laser and a 785 nm laser. The dynamic light scattering (DLS) results were measured on a Malvern Zetasizer Nano90 instrument.

Synthesis of FCDs

The FCDs were synthesized *via* hydrothermal reaction of citric acid and ethylenediamine in water, following a well-developed approach in a previous literature report.[37] Briefly, 2 mmol citric acid was dissolved in 10 mL water, and then mixed with 536 μL ethylenediamine under stirring for 10 min. The mixture solution was transferred into a 30 mL Teflon lined stainless-steel reactor and heated at 200 °C for 5 h. After that, the reactors were cooled to room temperature, and the obtained brown-black product was subjected to dialysis against water in a 12–14 kDa cut-off cellulose membrane for 48 h, to remove the excess reactants. The final product of a solid mass of FCDs was collected by freeze drying treatment.

Fluorescence spectra measurements

The system for one-photon fluorescence spectra measurement is shown in Fig. S17 (ESI†), in which a continuous wave (CW) laser beam was focused onto a cuvette containing an aqueous dispersion of FCDs *via* a lens (focal length: 10 cm). The fluorescence emission of the FCDs was collected perpendicular to the propagation direction of the incident laser by an objective (XLUMPlanFLN, 20 × 1.00 NA, Olympus), and recorded with an optical fibre spectrometer (for visible spectra measurements: PG2000, Ideaoptics, China; and for SWIR spectra measurements: NIR1700, Ideaoptics, China) after passing through a long-pass filter. For two-photon fluorescence spectra measurement, the optical setup was similar. The differences were that fs pulsed lasers (Mira-OPO, Coherent, Inc., 80 MHz, 200 fs for 760 nm to 1360 nm excitation. FLCPA-01C, Calmar Laser, 1 MHz, 400 fs for 1560 nm excitation) were used as the excitation sources and a short-pass filter was coupled in front of the spectrometer (Fig. S18, ESI†). It should be noted that D_2O rather than H_2O was used as a dispersion medium for FCDs, to avoid water absorption of SWIR excitation light.

THG spectra measurement

As shown in Fig. S19 (ESI†), the beam from a 1560 nm fs laser was coupled into an infrared antireflection objective (XLPLN25XWMP2, 25 × 1.05 NA, Olympus) to achieve high-intensity excitation towards the FCD sample. The excited THG signals were collected by another objective (10 × 0.25 NA) and recorded using the optical fiber spectrometer (PG2000, Ideaoptics, China), after passing through a short-pass filter. This system could work well, due to the excellent forward propagation characteristics of THG signals.

SWIR fluorescence imaging

As shown in Fig. S20 (ESI†), a laser beam with a wavelength of 785 nm/915 nm/980 nm was coupled with an optical collimator and expended by a lens to provide uniform illumination in the irradiation area. An electronic-cooling two-dimensional (640 pixels × 512 pixels) InGaAs camera (TEKWIN SYSTEM, China) equipped with a prime lens (focal length: 50 mm, Edmund Optics) with antireflection (AR) coating at 800–2000 nm was fixed 40 cm away from the irradiated area. A long-pass filter was mounted in front of the lens (950 nm long-pass for 785 nm excitation, 1000 nm long-pass for 915 nm excitation, 1100 nm long-pass for 980 nm excitation). The treated mice or centrifuge tubes filled with FCDs were placed in the irradiation area for SWIR fluorescence imaging.

Two-photon fluorescence microscopy

As shown in Fig. S21 (ESI†), the 1040 nm fs laser beam was coupled into an existing upright scanning microscope (BX61+FV1200, Olympus). The beam was reflected by a mirror, and then scanned by two computer-driven galvanometers. It further passed through a scan lens and a tube lens, and was focused onto the sample with a water-immersed microscope objective (XLUMPlanFLN, 20 × 1.00 NA, Olympus). Two-photon fluorescence signals were epi-collected with the same objective. They were extracted from the residual excitation laser with a dichroic mirror (DC) and a short-pass filter, and finally collected using a photomultiplier tube (PMT) for computer processing.

Two-photon fluorescence and THG microscopy based on the excitation of a 1560 nm fs laser

A similar optical setup to the aforementioned two-photon fluorescence microscope was used, by changing the excitation source to a 1560 nm fs laser. The THG and two-photon fluorescence signals from FCDs were collected by the same objective lens, and directed into two different channels by a dichroic mirror (570 nm, long-wavelength transmission and short-wavelength reflection) and an optical filter (495–540 nm bandpass) in the THG channel (THG channel: 495–540 nm; two-photon fluorescence channel: 570–800 nm, according to the detection range of the PMT).

Zebrafish culture and treatment

The zebrafish fish line (wild type AB line) was raised and maintained in the Zebrafish Resource Center (Core facilities, School of medicine, Zhejiang University), as described in our previous work.[57,58] Briefly, fish were seeded based on a constant 14 hour-on/10 hour-off light cycle while keeping the temperature at 28 °C. For toxicity assessment and bioimaging, 10 ng FCDs in 0.5 nL aqueous dispersion was microinjected into the yolk of a zebrafish embryo during the single-cell stage. In the control group, PBS was microinjected into the yolk of the embryo.

The treated fish were imaged using the aforementioned lab-built upright two-photon fluorescence scanning microscope (BX61+FV1200, Olympus) equipped with a 1040 nm fs laser.

Mouse culture and treatment

8 week-aged male nude mice were obtained from the Laboratory Animal Center of Zhejiang University (Hangzhou, China). The mice were housed in cages in several groups (5 mice per cage) and fed with standard mouse chow and water. The cages were maintained in a room with controlled temperature (25 ± 1 °C) and a 12 h light/dark cycle. The protocol of the animal experiments was approved by the Institutional Ethical Committee of Animal Experimentation of Zhejiang University in China, and the experiments were performed strictly according to governmental and international guidelines on animal experimentation. According to requirements for Biosafety and Animal Ethics, all efforts were made to minimize the number of animals used and their suffering.

For *in vivo* SWIR fluorescence imaging of the sentinel node, mice were anesthetized with pentobarbital, and 20 μL FCDs in PBS dispersion was injected through the forelegs. The treated mice were then exposed to 785 nm light excitation, and the InGaAs camera was used to capture the SWIR fluorescence images.

For *in vivo* SWIR fluorescence imaging of tumours, subcutaneous tumour bearing mice were anesthetized with pentobarbital, and 50 μL FCDs in PBS dispersion was used for intratumor injection. The administered mice were then excited with 915- and 980 nm lasers respectively, and the InGaAs camera was used to record the SWIR fluorescence images.

For *in vivo* two-photon fluorescence imaging, mice were anesthetized with pentobarbital, and the skulls of the mice were opened up through microsurgery. The meninges of the mice were punctured by syringe needles and the brains were incubated with a PBS dispersion of FCDs for 15 minutes. The brains were then carefully cleaned with normal saline. A metal ring with a handle was mounted onto the mouse brain. A round thin cover glass slide was then embedded in the metal ring and directly adhered to the mouse brain through dental cement. The brain was flattened by the cover glass slide, which was helpful to improve the microscopic imaging quality. The metal ring was then connected to a heavy metal plate with a handle, *via* handle-handle fix, which could keep the mouse's head immobilized during the whole imaging process. The aforementioned lab-built upright two-photon fluorescence scanning microscope (BX61+FV1200, Olympus) equipped with a 1040 nm fs laser was then used to perform the brain imaging.

For the metabolism and toxicity study, 30 days after the injection of FCDs, experimental mice, as well as control mice (without FCDs injection), were sacrificed. Their major organs (heart, liver, spleen, lungs, kidneys) were removed for histological analysis. Tissue samples were harvested and fixed in 4% para-formaldehyde overnight at 4 °C. Then the samples were embedded in paraffin, sectioned, and observed under a confocal fluorescence microscope (with a 20× objective lens). Finally, the histological sections were stained with H&E and imaged under an inverted optical microscope (with a 10× Objective lens).

Conflicts of interest

There are no conflicts to declare.

Acknowledgements

This work was supported by the National Natural Science Foundation of China (61735016), the Zhejiang Provincial Natural Science Foundation of China (LR17F050001), and National Basic Research Program of China (973 Program; 2013CB834704).

References

1 Y. P. Sun, B. Zhou, Y. Lin, W. Wang, K. A. S. Fernando, P. Pathak, M. J. Meziani, B. A. Harruff, X. Wang, H. F. Wang, P. J. G. Luo, H. Yang, M. E. Kose, B. L. Chen, L. M. Veca and S. Y. Xie, *J. Am. Chem. Soc.*, 2006, **128**, 7756–7757.
2 S. N. Baker and G. A. Baker, *Angew. Chem., Int. Ed.*, 2010, **49**, 6726–6744.
3 X. W. He and N. Ma, *Colloids Surf., B*, 2014, **124**, 118–131.
4 Y. Q. Zhang, D. K. Ma, Y. G. Zhang, W. Chen and S. M. Huang, *Nano Energy*, 2013, **2**, 545–552.
5 X. Guo, C. F. Wang, Z. Y. Yu, L. Chen and S. Chen, *Chem. Commun.*, 2012, **48**, 2692–2694.
6 K. Hola, Y. Zhang, Y. Wang, E. P. Giannelis, R. Zboril and A. L. Rogach, *Nano Today*, 2014, **9**, 590–603.
7 T. T. Sun, M. Zheng, Z. G. Xie and X. B. Jinga, *Mater. Chem. Front.*, 2017, **1**, 354–360.
8 Z. Liu, Q. Xu, Y. H. Li and W. Chen, *Mater. Chem. Front.*, 2017, **1**, 538–541.
9 N. Parvin, Q. Jin, Y. Z. Wei, R. B. Yu, B. Zheng, L. Huang, Y. Zhang, L. H. Wang, H. Zhang, M. Y. Gao, H. J. Zhao, W. P. Hu, Y. L. Li and D. Wang, *Adv. Mater.*, 2017, **29**, 1060755.
10 L. L. Pan, S. Sun, A. D. Zhang, K. Jiang, L. Zhang, C. Q. Dong, Q. Huang, A. G. Wu and H. W. Lin, *Adv. Mater.*, 2015, **27**, 7782–7787.
11 T. Feng, X. Z. Ai, G. H. An, P. P. Yang and Y. L. Zhao, *ACS Nano*, 2016, **10**, 4410–4420.
12 M. Zheng, S. Ruan, S. Liu, T. Sun, D. Qu, H. Zhao, Z. Xie, H. Gao, X. Jing and Z. Sun, *ACS Nano*, 2015, **9**, 11455–11461.
13 W. G. Kong, H. Z. Wu, Z. Y. Ye, R. F. Li, T. N. Xu and B. P. Zhang, *J. Lumin.*, 2014, **148**, 238–242.
14 M. Zheng, S. Liu, J. Li, Z. G. Xie, D. Qu, X. Miao, X. B. Jing, Z. C. Sun and H. Y. Fan, *J. Mater. Res.*, 2015, **30**, 3386–3393.
15 X. Y. Zhai, P. Zhang, C. J. Liu, T. Bai, W. C. Li, L. M. Dai and W. G. Liu, *Chem. Commun.*, 2012, **48**, 7955–7957.
16 H. Q. Tao, K. Yang, Z. Ma, J. M. Wan, Y. J. Zhang, Z. H. Kang and Z. Liu, *Small*, 2012, **8**, 281–290.
17 G. Hong, Y. Zou, A. L. Antaris, S. Diao, D. Wu, K. Cheng, X. Zhang, C. Chen, B. Liu, Y. He, J. Z. Wu, J. Yuan, B. Zhang, Z. Tao, C. Fukunaga and H. Dai, *Nat. Commun.*, 2014, **5**, 4206.
18 J. T. Robinson, K. Welsher, S. M. Tabakman, S. P. Sherlock, H. Wang, R. Luong and H. Dai, *Nano Res.*, 2010, **3**, 779–793.
19 A. L. Antaris, H. Chen, K. Cheng, Y. Sun, G. Hong, C. Qu, S. Diao, Z. Deng, X. Hu, B. Zhang, X. Zhang, O. K. Yaghi,

Z. R. Alamparambil, X. Hong, Z. Cheng and H. Dai, *Nat. Mater.*, 2016, **15**, 235–242.
20 O. T. Bruns, T. S. Bischof, D. K. Harris, D. Franke, Y. Shi, L. Riedemann, A. Bartelt, F. B. Jaworski, J. A. Carr, C. J. Rowlands, M. W. B. Wilson, O. Chen, H. Wei, G. W. Hwang, D. M. Montana, I. Coropceanu, O. B. Achorn, J. Kloepper, J. Heeren, P. T. C. So, D. Fukumura, K. F. Jensen, R. K. Jain and M. G. Bawendi, *Nat. Biomed. Eng.*, 2017, **1**, 0056.
21 K. Welsher, S. P. Sherlock and H. J. Dai, *Proc. Natl. Acad. Sci. U. S. A.*, 2011, **108**, 8943–8948.
22 P. T. C. So, C. Y. Dong, B. R. Masters and K. M. Berland, *Annu. Rev. Biomed. Eng.*, 2000, **2**, 399–429.
23 D. Kobat, M. E. Durst, N. Nishimura, A. W. Wong, C. B. Schaffer and C. Xu, *Opt. Express*, 2009, **17**, 13354–13364.
24 H. M. Kim and B. R. Cho, *Chem. Rev.*, 2015, **115**, 5014–5055.
25 D. Kobat, N. G. Horton and C. Xu, *J. Biomed. Opt.*, 2011, **16**, 106014.
26 D. D. Li, Q. Zhang, X. C. Wang, S. L. Li, H. P. Zhou, J. Y. Wu and Y. P. Tian, *Dyes Pigm.*, 2015, **120**, 175–183.
27 N. S. Alexander, G. Palczewska, P. Stremplewski, M. Wojtkowski, T. S. Kern and K. Palczewski, *Biomed. Opt. Express*, 2016, **7**, 2671–2691.
28 J. Wang and J. Liu, *RSC Adv.*, 2016, **6**, 19662–19668.
29 D. Wang, L. Zhu, C. McCleese, C. Burda, J.-F. Chen and L. Dai, *RSC Adv.*, 2016, **6**, 41516–41521.
30 J. J. Huang, M. Z. Rong and M. Q. Zhang, *Phys. Chem. Chem. Phys.*, 2016, **18**, 4800–4806.
31 Q. Liu, B. D. Guo, Z. Y. Rao, B. H. Zhang and J. R. Gong, *Nano Lett.*, 2013, **13**, 2436–2441.
32 D. Wang, Z. Y. Wang, Q. Q. Zhan, Y. Pu, J. X. Wang, N. R. Foster and L. M. Dai, *Engineering*, 2017, **3**, 402–408.
33 L. L. Pan, S. Sun, L. Zhang, K. Jiang and H. W. Lin, *Nanoscale*, 2016, **8**, 17350–17356.
34 L. Cao, X. Wang, M. J. Meziani, F. S. Lu, H. F. Wang, P. J. G. Luo, Y. Lin, B. A. Harruff, L. M. Veca, D. Murray, S. Y. Xie and Y. P. Sun, *J. Am. Chem. Soc.*, 2007, **129**, 11318–11319.
35 S. W. Wang, W. Xi, F. H. Cai, X. Y. Zhao, Z. P. Xu, J. Qian and S. L. He, *Theranostics*, 2015, **5**, 251–266.
36 Y. Wang, R. Hu, W. Xi, F. Cai, S. Wang, Z. Zhu, R. Bai and J. Qian, *Biomed. Opt. Express*, 2015, **6**, 3783–3794.
37 S. J. Zhu, Q. N. Meng, L. Wang, J. H. Zhang, Y. B. Song, H. Jin, K. Zhang, H. C. Sun, H. Y. Wang and B. Yang, *Angew. Chem., Int. Ed.*, 2013, **52**, 3953–3957.
38 J. G. Zhou, C. Booker, R. Y. Li, X. T. Zhou, T. K. Sham, X. L. Sun and Z. F. Ding, *J. Am. Chem. Soc.*, 2007, **129**, 744–745.
39 Y. Li, Y. Zhao, H. H. Cheng, Y. Hu, G. Q. Shi, L. M. Dai and L. T. Qu, *J. Am. Chem. Soc.*, 2012, **134**, 15–18.
40 Z. Wang, Y. Pu, D. Wang, J. Shi, J.-X. Wang and J.-F. Chen, *AIChE J.*, 2018, **64**, 1330–1338.
41 X. Jin, X. Sun, G. Chen, L. Ding, Y. Li, Z. Liu, Z. Wang, W. Pan, C. Hu and J. Wang, *Carbon*, 2015, **81**, 388–395.
42 S. J. Zhu, Q. N. Meng, L. Wang, J. H. Zhang, Y. B. Song, H. Jin, K. Zhang, H. C. Sun, H. Y. Wang and B. Yang, *Angew. Chem., Int. Ed.*, 2013, **52**, 3953–3957.
43 M. J. Krysmann, A. Kelarakis, P. Dallas and E. P. Giannelis, *J. Am. Chem. Soc.*, 2012, **134**, 747–750.
44 D. Qu, M. Zheng, P. Du, Y. Zhou, L. Zhang, D. Li, H. Tan, Z. Zhao, Z. Xie and Z. Sun, *Nanoscale*, 2013, **5**, 12272–12277.
45 T. Feng, X. Ai, G. An, P. Yang and Y. Zhao, *ACS Nano*, 2016, **10**, 4410–4420.
46 Z. Tao, X. Dang, X. Huang, M. D. Muzumdar, E. S. Xu, N. M. Bardhan, H. Song, R. Qi, Y. Yu, T. Li, W. Wei, J. Wyckoff, M. J. Birrer, A. M. Belcher and P. P. Ghoroghchian, *Biomaterials*, 2017, **134**, 202–215.
47 N. Li, X. F. Liang, L. L. Wang, Z. H. Li, P. Y. Li, Y. H. Zhu and J. Song, *J. Nanopart. Res.*, 2012, **14**, 1177.
48 T. Feng, X. Z. Ai, G. H. An, P. P. Yang and Y. L. Zhao, *ACS Nano*, 2016, **10**, 5587.
49 G. S. Hong, S. O. Diao, A. L. Antaris and H. J. Dai, *Chem. Rev.*, 2015, **115**, 10816–10906.
50 J. Qi, C. W. Sun, A. Zebibula, H. Q. Zhang, R. T. K. Kwok, X. Y. Zhao, W. Xi, J. W. Y. Lam, J. Qian and B. Z. Tang, *Adv. Mater.*, 2018, **30**, 1706856.
51 S. H. Li, Z. L. Peng, J. Dallman, J. Baker, A. M. Othman, P. L. Blackwelder and R. M. Leblanc, *Colloids Surf., B*, 2016, **145**, 251–256.
52 X. Han, Z. F. Jing, W. Wu, B. Zou, Z. L. Peng, P. Y. Ren, A. Wikramanayake, Z. M. Lu and R. M. Leblanc, *Nanoscale*, 2017, **9**, 12862–12866.
53 J. Qian, Z. F. Zhu, A. J. Qin, W. Qin, L. L. Chu, F. H. Cai, H. Q. Zhang, Q. Wu, R. R. Hu, B. Z. Tang and S. L. He, *Adv. Mater.*, 2015, **27**, 2332–2339.
54 A. Islam, E. I. Romijn, M. B. Lilledahl and I. Martinez-Zubiaurre, *Osteoarthritis and Cartilage*, 2017, **25**, 1729.
55 J. Su, J. Zhang, X. H. Tian, M. Zhao, T. Song, J. C. Yu, Y. J. Cui, G. D. Qian, H. Zhong, L. Luo, Y. J. Zhang, C. K. Wang, S. L. Li, J. X. Yang, H. P. Zhou, J. Y. Wu and Y. P. Tian, *J. Mater. Chem. B*, 2017, **5**, 5458–5463.
56 K. Kieu, S. Mehravar, R. Gowda, R. A. Norwood and N. Peyghambarian, *Biomed. Opt. Express*, 2013, **4**, 2187–2195.
57 N. Billington, J. R. Beach, S. M. Heissler, K. Remmert, S. Guzik-Lendrum, A. Nagy, Y. Takagi, L. Shao, D. Li, Y. Yang, Y. Zhang, M. Barzik, E. Betzig, J. A. Hammer 3rd and J. R. Sellers, *Curr. Biol.*, 2015, **25**, 942–948.
58 D. Y. Li, X. Y. Zhao, W. Qin, H. Q. Zhang, Y. Fei, L. W. Liu, K. T. Yong, G. D. Chen, B. Tang and J. Qian, *Nano Res.*, 2016, **9**, 1921–1933.

